Inorg. Chem. **2006**, *45*, 10520–10529

New Ru Complexes Containing the N-Tridentate bpea and Phosphine Ligands: Consequences of Meridional vs Facial Geometry

Joaquim Mola, Montserrat Rodríguez, and Isabel Romero*

Departament de Química, Universitat de Girona, Campus de Montilivi, E-17071 Girona, Spain

Antoni Llobet*,†

Departament de Química, Universitat Autònoma de Barcelona, Bellaterra, E-08193 Barcelona, Spain

Teodor Parella

Servei de RMN, Universitat Autònoma de Barcelona, Bellaterra, E-08193 Barcelona, Spain

Albert Poater, Miquel Duran, and Miquel Solà*

Institut de Química Computacional, Universitat de Girona, Campus de Montilivi, E-17071 Girona, Spain

Jordi Benet-Buchholz

Institut Català d'Investigació Química (ICIQ), Avgda. Països Catalans 16, E-43007 Tarragona, Spain

Received June 21, 2006

The synthesis and isolation of the complex *cis,fac*-[$Ru^{II}Cl_2$(bpea)(PPh_3)] [**3**; bpea = *N*,*N*-bis(2-pyridylmethyl)ethylamine] and three geometrical isomers of the complex [Ru^{II}Cl(bpea)(dppe)](BF_4) [**4**; dppe = (1,2-diphenylphosphino)ethane], *trans,fac* (**4a**), *cis,fac* (**4b**), and *mer(down)* (**4c**), have been described (see Chart 1 for a drawing of their structures). These complexes have been characterized through analytical, spectroscopic (IR, UV/vis, and 1D and 2D NMR), and electrochemical (cyclic voltammetry) techniques. In addition, complexes **3**, **4a**, and **4b** have been further characterized in the solid state through monocrystal X-ray diffraction analysis. The molecular and electronic structures of isomers **4a**, **4b**, **4c**, and **4d** (the *mer(up)* isomer) have also been studied by means of density functional theory (DFT) calculations. Furthermore, their low-energy electronic transitions have been simulated using time-dependent DFT approaches, which have allowed unraveling of their metal-to-ligand charge-transfer nature. Complexes **3** and **4a**–**c** are capable of catalyzing H-transfer types of reactions between alcohols and aromatic ketones such as acetophenone and 2,2-dimethylpropiophenone (DP). A strong influence of the facial versus meridional geometry in the bpea ligand coordination mode is observed for these catalytic reactions, with the meridional isomer being much more active than the facial one. The meridional isomer is even capable of carrying out the H-transfer reaction of bulky substrates such as DP at room temperature.

Introduction

Ru complexes are gathering a great deal of attention because of their multiple applications in many fields of science.[1] In particular, they are being used extensively as catalysts for a myriad of different processes including oxidative and reductive reactions.[2] In the field of catalysis by transition-metal complexes, the ligands attached to the metal center play a key role. The appropriate ligands allow for control of the steric and electronic properties and thus governance of the catalyst performance in terms of selectivity and efficiency. Therefore, the design of new ligands to adequately influence the reactivity is one of the most important challenges nowadays in this field.[3]

* To whom correspondence should be addressed. E-mail: marisa.romero@udg.es (I.R.), allobet@ICIQ.es (A.L.), miquel.sola@udg.es (M.S.).

† Also at Institut Català d'Investigació Química (ICIQ), Avgda. Països Catalans 16, E-43007 Tarragona, Spain.

10.1021/ic061126l CCC: $33.50
Published on Web 11/22/2006

Ru(II) complexes containing tertiary phosphines have been extensively studied from a synthetic viewpoint, and their performance as catalysts is well-known.[4] More recently, there has been an increased interest in mixed-ligand complexes containing both phosphine types of donors and also N types of donors such as amines and aromatic N-heterocyclic ligands as a result of the unique electronic properties that this combination of ligands is able to transmit to the metal center.[5]

With the aim of contributing to the understanding of how geometric and electronic factors imposed by a combination of mixed ligands (N and P types), influence the catalyst performance, we have prepared a family of Ru(II)−Cl complexes bearing the N-tridentate *N*,*N*-bis(2-pyridylmethyl)ethylamine (bpea) ligand and the P-bidentate (1,2-diphenylphosphino)ethane (dppe) ligand. This family of Ru−Cl complexes has been thoroughly characterized, and its catalytic performance has been tested with regard to the transfer hydrogenation of aromatic ketone reaction.

Experimental Section

Materials. All reagents used in the present work were obtained from Aldrich Chemical Co. and were used without further purification. Reagent-grade organic solvents were obtained from SDS, and high-purity deionized water was obtained by passing distilled water through a nanopure Milli-Q water purification system. $RuCl_3 \cdot 3H_2O$ was supplied by Johnson and Matthey Ltd. and was used as received. MeOH (p.a. 99%, Scharlau) was used without further purification.

Preparations. The bpea ligand[6] and complexes $Ru^{II}Cl_2(PPh_3)_3$ (**1**)[7] and $Ru^{III}Cl_3(bpea) \cdot 2H_2O$ (**2**·$2H_2O$)[8] were prepared according to literature procedures. All synthetic manipulations were routinely performed under a N_2 atmosphere using Schlenck tubes and vacuum-line techniques.

$Ru^{II}Cl_2(bpea)(PPh_3) \cdot 4H_2O$ (3·$4H_2O$). A solution of bpea (95 mg, 0.417 mmol) and **1** (400 mg, 0.417 mmol) in 50 mL of anhydrous tetrahydrofuran was refluxed for 1 h, under a N_2 atmosphere. Upon cooling to room temperature, an orange solid precipitated. The solid was isolated by filtration, washed with hexane (to remove free phosphine) and ether, and dried under vacuum. Yield: 0.25 g (90%). Anal. Found (calcd) for $C_{32}H_{32}Cl_2N_3PRu \cdot 4H_2O$: C, 52.21 (52.38); H, 5.24 (5.49); N, 5.42 (5.72). IR (cm^{-1}): ν 3600−3200, 3048, 2922, 1480, 1433, 1087, 696 cm^{-1}. ^1H NMR (CD_2Cl_2, 500 MHz, 25 °C): δ 8.11 (m, 6, H_{16A}, H_{20A}, H_{22A}, H_{26A}, H_{28A}, H_{32A}), 7.46 (m, 2, H_{1A}, H_{14A}), 7.38 (m, 6, H_{17A}, H_{19A}, H_{23A}, H_{25A}, H_{29A}, H_{31A}), 7.34 (m, 3, H_{18A}, H_{30A}, H_{24A}), 7.06 (m, 2, H_{3A}, H_{12A}), 7.02 (d, $^3J_{4A-5A}$ = 6.5 Hz, 2, H_{4A}, H_{11A}), 6.32 (m, 2, H_{2A}, H_{13A}), 5.06 (d, $^3J_{6Ab-6Aa}$ = 14.55 Hz, 2, H_{6Ab}, H_{9Ab}), 4.38 (m, 2, H_{7A}), 4.15 (d, $^3J_{6Aa-6Ab}$ = 14.55 Hz, 2, H_{6Aa}, H_{9Aa}), 1.45 (t, $^3J_{8A-7A}$ = 7.2 Hz, 3, H_{8A}). ^{13}C NMR (CD_2Cl_2, 500 MHz, 190 K): δ 157.6 (C_{1A}, C_{14A}), 135.4 (C_{16A}, C_{20A}, C_{22A}, C_{26A}, C_{28A}, C_{32A}), 134 (C_{3A}, C_{12A}), 128.7 (C_{17A}, C_{19A}, C_{23A}, C_{25A}, C_{29A}, C_{31A}), 128.0 (C_{18A}, C_{30A}, C_{24A}), 121.1 (C_{2A}, C_{13A}), 120 (C_{4A}, C_{11A}), 65.2 (C_{6A}, C_{9A}), 55.2 (C_{7A}), 7.25 (C_{8A}). NOE: H_{4A} with H_{6Aa}. ^{31}P NMR (CD_2Cl_2, 202 MHz, 180 K): δ 56 (s). $E_{1/2}$ (V; CH_2Cl_2 + 0.1 M TBAP): 0.30 vs SSCE. UV/vis [CH_2Cl_2; λ_{max}/nm (ϵ/M^{-1} cm^{-1})]: 232 (23 273), 361 (sh), 399 (4628), 484 (sh).

For the NMR assignments of **3**, **4a**, and **4b**, we use the same labeling scheme as that used in the crystal structures shown in Figure 1. For **4c**, we use the labeling scheme of the calculated structure shown in the Supporting Information.

[Ru^{II}Cl(bpea)(dppe)](BF_4) (4). A sample of $Ru^{III}Cl_3(bpea) \cdot 2H_2O$ (100 mg, 0.23 mmol) and LiCl (30 mg, 0.69 mmol) was dissolved in a 3:1 EtOH/H_2O mixture (40 mL) under a N_2 atmosphere. Then NEt_3 (0.05 mL, 0.345 mmol) was added, and the brown mixture was stirred for 15 min at room temperature, upon which it progressively became a dark-green solution. At this point, the dppe ligand (91 mg, 0.69 mmol) dissolved in 2 mL of EtOH was added, and the resulting solution was maintained at reflux for 3.5 h. Upon cooling to room temperature, the volume was reduced at low pressure up to 20 mL and the solution filtered on a frit to eliminate small amounts of a dark-brown solid. Afterward, 2 mL of a saturated aqueous solution of $NaBF_4$ was added to the solution, and the mixture was extracted with CH_2Cl_2. The organic phase was then dried over anhydrous $MgSO_4$ and the volume of the solution removed under reduced pressure. A green solid was obtained, which was purified by flash chromatography on a silica column. Elution with 8:1 CH_2Cl_2/CH_3CN allows one to obtain a mixture of *trans*,*fac*-[Ru^{II}Cl(bpea)(dppe)](BF_4) (**4a**) and *cis*,*fac*-[Ru^{II}Cl(bpea)(dppe)](BF_4) (**4b**). Further elution with 16:8:1 CH_2Cl_2/CH_3CN/MeOH allows one to obtain the *mer(down)*-[Ru^{II}Cl(bpea)(dppe)](BF_4) isomer, **4c**. The first two isomers were then separated using a silica preparative plate (eluent 9:1 CH_2Cl_2/acetone) to yield **4a** and **4b** as bright-yellow solids.

Isomer 4a·$3H_2O$. Yield: 57 mg (27.8%). Anal. Found (calcd) for $C_{40}H_{41}BClF_4N_3P_2Ru \cdot 3H_2O$: C, 53.30 (53.20); H, 5.29 (5.25); N, 4.95 (4.65). ^1H NMR (CD_2Cl_2, 500 MHz, 25 °C): δ 9.63 (dt, $^3J_{5-4}$ = 5.4 Hz, $^3J_{5-P}$ = 1.5 Hz, $^3J_{5-3}$ = 1.5 Hz, 2, H_5, H_{12}), 7.80 (dt, $^3J_{3-2}$ = 7.8 Hz, $^3J_{3-4}$ = 7.8 Hz, $^3J_{3-5}$ = 1.5 Hz, 2, H_3, H_{10}), 7.53 (dd, $^3J_{22-23}$ = 7.5 Hz, $^3J_{22-P}$ = 8.4 Hz, 4, H_{22}, H_{26}, H_{36}, H_{40}),

(1) (a) Ballardini R.; Balzani, V.; Credi, A.; Gandolfi, M. T.; Venturi, M. *Int. J. Photoenergy* **2004**, *6*, 1−10. (b) Baranoff, E.; Collin, J.-P.; Furusho, J.; Furusho, Y.; Laemmel, A.-C.; Sauvage, J.-P. *Inorg. Chem.* **2002**, *41*, 1215−1222. (c) Weatherly, S. C.; Yang, I. V.; Thorp, H. H. *J. Am. Chem. Soc.* **2001**, *123*, 1236−1237. (d) Kelly, S. O.; Barton, J. K. *Science* **1999**, *238*, 375−381. (e) Schuster, G. B. *Acc. Chem. Res.*. **2000**, *33*, 253−260.

(2) (a) Murahashi, S. I.; Takaya, H.; Naota, T. *Pure Appl. Chem.* **2002**, *74*, 19−24. (b) Naota, T.; Takaya, H.; Murahashi, S. I. *Chem. Rev.* **1998**, *98*, 2599−2660. (c) Riley, D. P.; Oliver, J. D. *Inorg. Chem.* **1986**, *25*, 1825−1830. (d) Rodríguez, M.; Romero, I.; Llobet, A.; Deronzier, A.; Biner, M.; Parella, T.; Stoeckli-Evans, H. *Inorg. Chem.* **2001**, *40*, 4150−4156. (e) Chronister, C. W.; Binstead, R. A.; Ni, J.; Meyer, T. J. *Inorg. Chem.* **1997**, *36*, 3814−3815. (f) Jauregui-Haza, U. J.; Dessoudeix, M.; Kalck, P.; Wilhelm, A. M.; Delmas, H. *Catal. Today* **2001**, *66*, 297−302.

(3) (a) *Opportunities for Catalysis in the 21st Century; A Report from the Basic Energy Sciences Advisory Committee*; U.S. Department of Energy: Washington, DC, 2002. (b) *Basic Research Needs for the Hydrogen Economy; A Report from the Basic Energy Sciences Workshop on Hydrogen Production, Storage and Use*; U.S. Department of Energy; Washington, DC, 2003.

(4) (a) Berthod, M.; Mignani, G.; Woodward, G.; Lemaire, M. *Chem. Rev.* **2005**, *105* (5), 1801−1836. (b) Xia, Q.-H.; Ge, H.-Q.; Ye, C. P.; Liu, Z. M.; Su, K.-X. *Chem. Rev.* **2005**, *105* (5), 1603−1662.

(5) (a) Rahman, M. S.; Prince, P. D.; Steed, J. W.; Hii, K. K. *Organometallics* **2002**, *21*, 4927−4933. (b) Braunstein, P.; Naud, F.; Pfaltz, A.; Rettig, S. J. *Organometallics* **2000**, *19*, 2676−2683. (c) Baratta, W.; Herdtweck, E.; Siega, K.; Toniutti, M.; Rigo, P. *Organometallics* **2005**, *24*, 1660−1669. (d) Danopoulos, A. A.; Winston, S.; Motherwell, W. B. *Chem. Commun.* **2002**, 1376−1377. (e) Ohkuma, T.; Sandoval, C. A.; Srinivasan, R.; Lin, Q.; Wei, Y.; Muniz, K.; Noyori, R. *J. Am. Chem. Soc.* **2005**, *127*, 8288−8289. (f) Cuervo, D.; Gamasa, M. P.; Gimeno, J. *Chem.—Eur. J.* **2004**, *10*, 425−432. (g) Rautenstrauch, V.; Hoang-Cong, X.; Churlaud, R.; Abdur-Rashid, K.; Morris, R. H. *Chem.—Eur. J.* **2003**, *9*, 4954−4967.

(6) Pal, S.; Chan, M. K.; Armstrong, W. H. *J. Am. Chem. Soc.* **1992**, *114*, 6398−6406.

(7) Hallman, P. S.; Stephenson, T. A.; Wilkinson, G. *Inorg. Synth.* **1970**, *12*, 237−240.

(8) Serrano, I.; Llobet, A.; Rodríguez, M.; Romero, I.; Benet-Buchholz, J.; Parella, T.; Luna, D.; Campelo, J. M.; Marinas, J. M. *Inorg. Chem.* **2006**, *45*, 2644−2651.

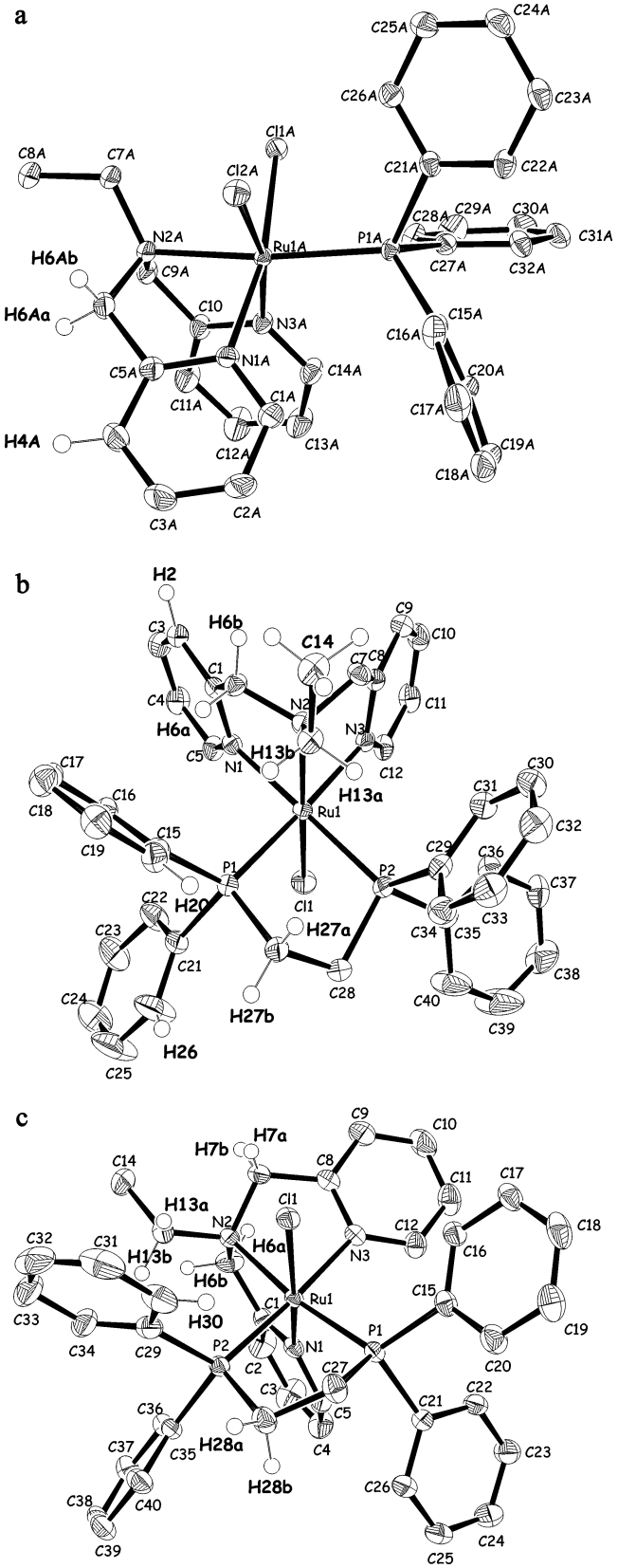

Figure 1. X-ray structure (ORTEP plots with ellipsoids at the 50% probability level) and labeling scheme for the cationic parts of (a) **3** (molecule A), (b) **4a**, and (c) **4b**.

7.40 (ddd, $^3J_{4-3}$ = 7.8 Hz, $^3J_{4-5}$ = 5.4 Hz, $^3J_{4-2}$ = 1.5 Hz, 2, H_4, H_{11}; m, 2, H_{24}, H_{38}), 7.38 (m, 2, H_{18}, H_{32}), 7.37 (dd, $^3J_{2-3}$ = 7.8 Hz, $^3J_{2-4}$ = 1.5 Hz, 2, H_2, H_9), 7.34 (m, 4, H_{16}, H_{20}, H_{31}, H_{34}), 7.31 (m, 4, H_{17}, H_{19}, H_{30}, H_{33}), 7.30 (td, $^3J_{23-22}$ = 7.5 Hz, $^3J_{23-24}$ = 7.5 Hz, $^3J_{23-P}$ = 1.4 Hz, 4, H_{23}, H_{25}, H_{37}, H_{39}), 3.91 (d, $^3J_{6a-6b}$ = 16.1 Hz, 2, H_{6b}, H_{7b}), 3.42 (d, $^3J_{6a-6b}$ = 16.1 Hz, 2, H_{6a}, H_{7a}), 3.21 (m, 2, H_{27a}, H_{28a}), 3.08 (m, 2, H_{27b}, H_{28b}), 2.25 (q, $^3J_{14-13}$ = 7 Hz, 2, H_{13}), 0.53 (t, $^3J_{14-13}$ = 7 Hz, 3, H_{14}). ^{13}C NMR (CD_2Cl_2, 500 MHz, 25 °C): δ 151.0 (C_5, C_{12}), 138.2 (C_3, C_{10}), 132.0 (C_{22}, C_{26}, C_{36}, C_{40}), 130.4 (C_{24}, C_{38}), 129.7 (C_{16}, C_{20}, C_{31}, C_{34}), 128.9 (C_{18}, C_{32}), 128.1 (C_{17}, C_{19}, C_{30}, C_{33}, C_{23}, C_{25}, C_{37}, C_{39}), 124.5 (C_4, C_{11}), 122.5 (C_2, C_9), 68.5 (C_6, C_7), 62.5 (C_{13}), 24.6 (C_{27}, C_{28}), 8.1 (C_{14}). ^{31}P NMR (CD_2Cl_2, 202 MHz, 25 °C): δ 57.7 (s). NOEs: H_{13b} with H_{27a}, H_{6a}; H_{6b} with H_{14}, H_{6a}, H_2; H_{27a} with H_{20}; H_{27b} with H_{26}. $E_{1/2}$ (V; CH_2Cl_2 + 0.1 M TBAP): 1.10 vs SSCE. UV/vis [CH_2Cl_2; λ_{max}/nm (ϵ/M^{-1} cm^{-1})]: 238 (27 567), 267 (4684), 303 (5936), 334 (5710).

Isomer 4b·2.5H_2O. Yield: 32 mg (15.6%). Anal. Found (calcd) for $C_{40}H_{41}BClF_4N_3P_2Ru$·2.5$H_2O$: C, 53.46 (53.73); H, 5.32 (5.18); N, 4.95 (4.69). ^{1}H NMR (CD_2Cl_2, 500 MHz, 25 °C): δ 8.77 (d, $^3J_{12-P2}$ = 1.7 Hz, 1, H_{12}), 7.77 (dd, 2, H_{22}, H_{26}), 7.73 (t, 1, H_{10}), 7.67 (dd, 2, H_{30}, H_{34}), 7.54 (d, 1, H_9), 7.49 (t, 1, H_{18}), 7.46 (m, 2, H_{24}, H_{32}), 7.45 (t, 1, H_{38}), 7.38 (t, 2, H_{31}, H_{33}), 7.34 (t, 2, H_{17}, H_{19}), 7.33 (m, 3, H_3, H_{23}, H_{25}), 7.24 (t, 2, H_{37}, H_{39}), 7.14 (d, 2, H_{16}, H_{20}), 7.12 (d, 1, H_2), 6.98 (t, 1, H_{11}), 6.95 (dt, $^3J_{40-P1}$ = 8.5 Hz, $^3J_{40-39}$ = 7.5 Hz, $^3J_{40-38}$ = 1.5 Hz, 2, H_{36}, H_{40}), 6.55 (d, $^3J_{5-P1}$ = 1.5 Hz, 1, H_5), 6.09 (t, 1, H_4), 5.04 (d, $^3J_{7a-7b}$ = 14.6 Hz, 1, H_{7a}), 4.41 (s, 2, H_6), 4.34 (dd, $^3J_{7b-7a}$ = 14.6 Hz, $^3J_{7b-P1}$ = 3.7 Hz, 1, H_{7b}), 3.79 (m, $^3J_{13b-13a}$ = 14.2 Hz, 1, H_{13a}), 3.21 (m, 1, H_{27a}), 3.11 (m, 1, H_{28b}), 2.98 (m, 1, H_{27b}), 2.94 (m, 1, H_{28a}), 2.65 (q, $^3J_{13b-13a}$ = 14.2 Hz, $^3J_{13b-14}$ = 7.1 Hz, 1, H_{13b}), 1.12 (t, $^3J_{14-13}$ = 7.1 Hz, 3, H_{14}). ^{13}C NMR (CD_2Cl_2, 500 MHz, 25 °C): δ 155.1 (C_{12}), 136.1 (C_{22}, C_{26}), 133.3 (C_{30}, C_{34}), 132.7 (C_{16}, C_{20}), 132 (C_{36}, C_{40}), 130.6 (C_{18}, C_{24}, C_{32}, C_{38}), 130.4 (C_{23}, C_{25}, C_{31}, C_{33}), 130.3 (C_{17}, C_{19}), 129.3 (C_{37}, C_{39}), 124 (C_{11}), 123.3 (C_4), 122.5 (C_9, C_{10}), 121.8 (C_2), 66.1 (C_7), 65.8 (C_6), 60.3 (C_{13}), 29.9 (C_{28}), 28.2 (C_{27}), 8.3 (C_{14}). ^{31}P NMR (CD_2Cl_2, 202 MHz, 25 °C): δ 70.7 (d, $^2J_{P1-P2}$ = 7.45 Hz, P_1), 61.6 (d, P_2). NOEs: H_{13a} with H_{30}, H_{7a}; H_{13b} with H_6; H_{28a} with H_{30}. $E_{1/2}$ (V; CH_2Cl_2 + 0.1 M TBAP): 1.10 vs SSCE. UV/vis [CH_2Cl_2; λ_{max}/nm (ϵ/M^{-1} cm^{-1})]: 233 (18 198), 238 (sh), 276 (5765), 343 (2180), 392 (sh).

Isomer 4c·EtOH. Yield: 17 mg (8.33%). Anal. Found (calcd) for $C_{40}H_{41}BClF_4N_3P_2Ru$·EtOH: C, 56.40 (56.36); H, 5.12 (5.29); N, 4.72 (4.69). ^{1}H NMR (CD_2Cl_2, 500 MHz, 25 °C): δ 8.13 (dd, $^3J_{20-21}$ = 8 Hz, $^3J_{20-P}$ = 8 Hz, 4, H_{20}, H_{26}, H_{36}, H_{40}), 7.58 (d, $^3J_{2-3}$ = 4.2 Hz, 2, H_2, H_9), 7.58 (d, 2, H_3, H_{10}), 7.32 (m, 2, H_{22}, H_{38}), 7.30 (m, 4, H_{21}, H_{25}, H_{37}, H_{39}), 7.24 (t, 2, H_{18}, H_{32}), 7.15 (d, $^3J_{5-4}$ = 5.7 Hz, 2, H_5, H_{12}), 7.05 (t, 4, H_{17}, H_{23}, H_{31}, H_{33}), 6.61 (dd, $^3J_{16-17}$ = 7.5 Hz, $^3J_{16-P}$ = 7.5 Hz, 4, H_{16}, H_{24}, H_{30}, H_{34}), 6.43 (ddd, $^3J_{3-2}$ = 7.5 Hz, $^3J_{3-4}$ = 7.4 Hz, $^3J_{3-5}$ = 1.5 Hz, 2, H_4, H_{11}), 5.94 (d, $^3J_{6a-6b}$ = 15.7 Hz, 2, H_{6a}, H_{7a}), 4.77 (dd, $^3J_{6b-6a}$ = 15.7 Hz, $^3J_{6b-P}$ = 3.8 Hz, 2, H_{6b}, H_{7b}), 3.08 (q, $^3J_{13-14}$ = 7 Hz, 2, H_{13}), 2.96 (m, 2, H_{28}), 2.89 (m, 2, H_{27}), 1.33 (t, $^3J_{14-13}$ = 7 Hz, 3, H_{14}). ^{13}C NMR ($CDCl_3$, 500 MHz, 25 °C): δ 165.4 (C_1, C_8), 156.9 (C_5, C_{12}), 137.5 (C_3, C_{10}), 133.9 (C_{19}, C_{35}), 132.9 (C_{20}, C_{26}, C_{36}, C_{40}), 131.2 (C_{16}, C_{24}, C_{30}, C_{34}), 130.4 (C_{18}, C_{32}), 130.3 (C_{22}, C_{38}), 130.2 (C_{15}, C_{29}), 129.1 (C_{17}, C_{23}, C_{31}, C_{33}), 128.9 (C_{21}, C_{25}, C_{37}, C_{39}), 123.3 (C_2, C_9), 122.9 (C_4, C_{11}), 60.4 (C_6, C_7), 59.5 (C_{13}), 30.6 (C_{27}), 24.8 (C_{28}), 9.4 (C_{14}). ^{31}P NMR ($CDCl_3$, 101 MHz, 25 °C): δ 60.8 (d, $^2J_{P1-P2}$ = 18.9 Hz, P_1), 59.5 (d, P_2). NOEs: H_5 with H_{20}, H_{6b} with H_{13}, H_2; H_{13} with H_{16}. $E_{1/2}$ (V; CH_2Cl_2 + 0.1 M TBAP): 1.21 vs SSCE. UV/vis [CH_2Cl_2; λ_{max}/nm (ϵ/M^{-1} cm^{-1})]: 243 (40 142), 275 (6308), 335 (sh), 371 (5499), 396 (6014).

Instrumentation and Measurements. Fourier transform IR (FT-IR) spectra were taken in a Mattson-Galaxy Satellite FT-IR spectrophotometer containing a MKII Golden Gate Single Reflec-

tion ATR system. UV/vis spectroscopy was performed on a Cary 50 Scan (Varian) UV/vis spectrophotometer with 1-cm quartz cells. Cyclic voltammetric (CV) experiments were performed in a PAR 263A EG&G potentiostat or an IJ-Cambria IH-660 using a three-electrode cell. Glassy-carbon disk electrodes (3-mm diameter) from BAS were used as working electrodes, platinum wire was used as the auxiliary electrode, and SSCE was used as the reference electrode. All cyclic voltammograms presented in this work were recorded under a N_2 atmosphere. All $E_{1/2}$ values reported in this work were estimated from CV as the average of the oxidative and reductive peak potentials $(E_{p,a} + E_{p,c})/2$ at a scan rate of 100 mV s^{-1}. The cyclic voltammograms were registered in CH_2Cl_2 containing 0.1 M TBAP. Under these conditions, the $E_{1/2}$ value for ferrocene is 0.430 V. Unless explicitly mentioned, the concentration of all of the complexes was approximately 1 mM. NMR spectroscopy was performed on a Bruker 500 MHz or a Bruker DPX 200 MHz. Samples were run in CD_2Cl_2 using tetramethylsilane and/or residual protons as the internal standard. Elemental analyses were performed using a CHNS−O Elemental Analyser EA-1108 from Fisons.

Catalytic Hydrogenation of Ketones. Experiments have been performed in 2-propanol as the source of reducing equivalents. In a typical run, Ru catalyst (0.62 mM), PhC(O)R (100 mM), $KOBu^t$ (50 mM), and biphenyl (15 mM) were stirred at 80 °C in 2-propanol (10 mL) for 24 h. Each aliquot was analyzed in a Shimadzu GC-17A gas chromatography (GC) apparatus equipped with a J&W Scientific β-cyclodex chiral column and a flame ionization detector, and quantification was achieved from calibration curves. GC conditions: initial temperature 80 °C for 10 min, ramp rate 10 °C min^{-1}, final temperature 220 °C, injection temperature 250 °C, detector temperature 300 °C, and carrier gas He at 25 mL min^{-1}. All catalytic hydrogenations were carried out under a N_2 atmosphere.

X-ray Structure Determination. Crystals of **3** were grown from dichloromethane as orange/brown blocks. Suitable crystals of **4a** and **4b** were grown respectively by crystallization at room temperature from CH_2Cl_2/diethyl ether as light-yellow plates and blocks. Measurement of the crystals was performed on a Siemens P4 diffractometer equipped with a SMART-CCD-1000 area detector, a MACScience Co. rotating anode with Mo Kα radiation, a graphite monochromator, and a Siemens low-temperature device LT2. Software: Data collection, *Smart*, version 5.060 (Bruker AXS, 1999); data reduction, *Saint+*, version 6.02 (Bruker AXS, 1999); absorption correction, *SADABS* (Bruker AXS, 1999); structure solution and refinement, *SHELXTL*, version 6.12 (Sheldrick, 2000).[9] The crystallographic data as well as details of the structure solution and refinement procedures are reported in Table 1. CCDC 602133−602135 contain the supplementary crystallographic data for this paper. These data can be obtained free of charge from the Cambridge Crystallographic Data Centre via www.ccdc.cam.ac.uk/data_request/cif.

Computational Details. The density functional theory (DFT) calculations have been carried out with the hybrid B3PW91 density functional,[10,11] as implemented in the *Gaussian 03* package.[12] The Ru atoms have been represented with the quasi relativistic effective core pseudopotentials (RECP) of the Stuttgart group and the associated basis sets augmented with an *f* polarization function (α = 1.235).[13,14] The remaining atoms (C, O, and H) have been represented with the 6-31G(d,p) basis set.[15] The B3PW91 geometry optimizations were performed without any symmetry constraints, and the nature of the minima was checked by analytical frequency calculations. The energies given throughout the paper are electronic energies without zero-point energy (ZPE) corrections (inclusion of the ZPE corrections does not significantly modify the results) or Gibbs free energy values computed at 298 K and 1 atm. TD-DFT calculations[16] at the same level of theory were performed to simulate UV/vis spectra. Finally, the dihedral angle between the best adjusted planes defined by two groups of atoms was measured by the *Spartan'02* program.[17]

Scheme 1. Synthetic Strategy

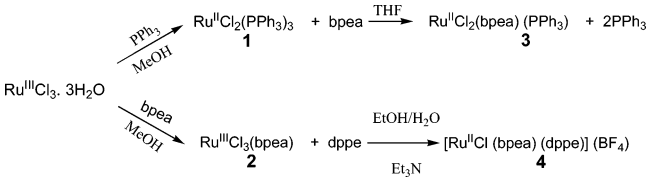

Results and Discussion

Synthesis and Crystal Structures. The synthetic strategy followed for the preparation of Ru^{II}−Cl complexes **3** and **4**, bearing both N and P types of ligands, is outlined in Scheme 1. $RuCl_3 \cdot 3H_2O$ is used as the starting material in any case, and then the N or P type of ligand is added stepwise. In the case of **3**, PPh_3 is added first, forming the synthetic intermediate **1**, and then the addition of bpea replaces two PPh_3 ligands, forming **3**. For complex **4**, the first ligand added is the N-type bpea to generate the synthetic intermediate **2**, followed by the reduction to Ru(II) and the addition of dppe, which replaces two of the three chloro ligands, to finally generate **4**. The bpea ligand is a sufficiently flexible tridentate ligand that can potentially coordinate in a meridional or a

(9) Sheldrick, G. M. *SHELXTL*, version 6.10; University of Göttingen: Göttingen, Germany, 2000.
(10) Becke, A. D. *J. Chem. Phys.* **1993**, *98*, 5648−5652.
(11) Perdew, J. P.; Wang, Y. *Phys. Rev. B* **1992**, *45*, 13244−13249.
(12) Frisch, M. J.; Trucks, G. W.; Schlegel, H. B.; Scuseria, G. E.; Robb, M. A.; Cheeseman, J. R.; Montgomery, J. A.; Vreven, T., Jr.; Kudin, K. N.; Burant, J. C.; Millam, J. M.; Iyengar, S. S.; Tomasi, J.; Barone, V.; Mennucci, B.; Cossi, M.; Scalmani, G.; Rega, N.; Petersson, G. A.; Nakatsuji, H.; Hada, M.; Ehara, M.; Toyota, K.; Fukuda, R.; Hasegawa, J.; Ishida, M.; Nakajima, T.; Honda, Y.; Kitao, O.; Nakai, H.; Klene, M.; Li, X.; Knox, J. E.; Hratchian, H. P.; Cross, J. B.; Bakken, V.; Adamo, C.; Jaramillo, J.; Gomperts, R.; Stratmann, R. E.; Yazyev, O.; Austin, A. J.; Cammi, R.; Pomelli, C.; Ochterski, J. W.; Ayala, P. Y.; Morokuma, K.; Voth, G. A.; Salvador, P.; Dannenberg, J. J.; Zakrzewski, V. G.; Dapprich, S.; Daniels, A. D.; Strain, M. C.; Farkas Ö.; Malick, D. K.; Rabuck, A. D.; Raghavachari, K.; Foresman, J. B.; Ortiz, J. V.; Cui, Q.; Baboul, A. G.; Clifford, S.; Cioslowski, J.; Stefanov, B. B.; Liu, G.; Liashenko, A.; Piskorz, P.; Komaromi, I.; Martin, R. L.; Fox, D. J.; Keith, T.; Al-Laham, M. A.; Peng, C. Y.; Nanayakkara, A.; Challacombe, M.; Gill, P. M. W.; Johnson, B.; Chen, W.; Wong, M. W.; Gonzalez, C.; Pople, J. A. *Gaussian 03*; Gaussian, Inc.: Pittsburgh, PA, 2004.
(13) Andrae, D.; Haussermann, U.; Dolg, M.; Stoll, H.; Preuss, H. *Theor. Chim. Acta* **1990**, *77*, 123−141.
(14) Bergner, A.; Dolg, M.; Kuchle, W.; Stoll, H.; Preuss, H. *Mol. Phys.* **1993**, *80*, 1431−1444.
(15) Hehre, W. J.; Ditchfield, R.; Pople, J. A. *J. Chem. Phys.* **1972**, *56*, 2257−2261.
(16) (a) Casida, M. E.; Jamorski, C.; Casida, K. C.; Salahub, D. R. *J. Chem. Phys.* **1998**, *108*, 4439−4449. (b) Stratmann, R. E.; Scuseria, G. E.; Frisch, M. J. *J. Chem. Phys.* **1998**, *109*, 8218−8224.
(17) Kong, J.; White, C. A.; Krylov, A. I.; Sherrill, C. D.; Adamson, R. D.; Furlani, T. R.; Lee, M. S.; Lee, A. M.; Gwaltney, S. R.; Adams, T. R.; Ochsenfeld, C.; Gilbert, A. T. B.; Kedziora, G. S.; Rassolov, V. A.; Maurice, D. R.; Nair, N.; Shao, Y.; Besley, N. A.; Maslen, P. E.; Dombroski, J. P.; Daschel, H.; Zhang, W.; Korambath, P. P.; Baker, J.; Byrd, E. F. C.; Van Voorhis, T.; Oumi, M.; Hirata, S.; Hsu, C.-P.; Ishikawa, N.; Florian, J.; Warshel, A.; Johnson, B. G.; Gill, P. M. W.; Head-Gordon, M.; Pople, J. A. *J. Comput. Chem.* **2000**, *21*, 1532−1548.

Chart 1. Possible Diastereoisomers for **4**

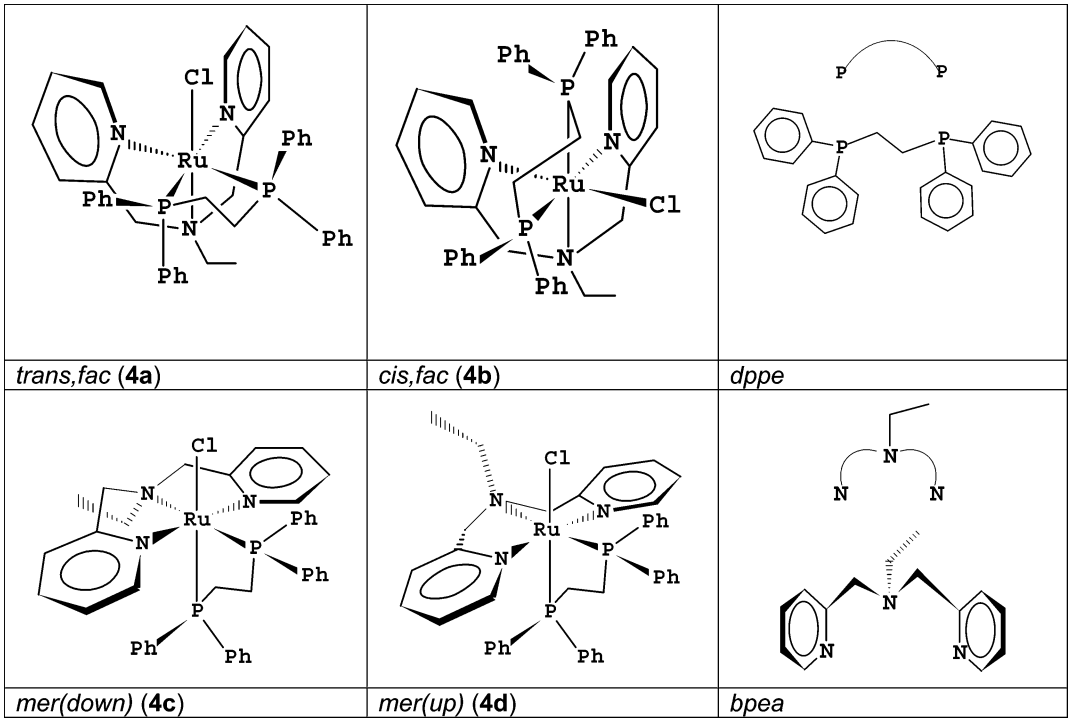

Table 1. Crystal Data for Complexes **3**, **4a**, and **4b**

	3	**4a**	**4b**
empirical formula	$C_{32}H_{32}Cl_2N_3P_1Ru_1 \times 2$	$C_{41}H_{43}BCl_3F_4N_3P_2Ru$	$C_{41}H_{43}BCl_3F_4N_3P_2Ru$
fw	1323.09	933.95	933.95
cryst syst, space group	monoclinic, $P2_1/c$	triclinic, $P\bar{1}$	monoclinic, $P2_1/n$
a [Å]	9.8333(4)	9.1355(6)	13.5744(2)
b [Å]	17.9544(7)	11.7412(8)	17.3626(3)
c [Å]	33.2513(14)	20.6366(14)	17.5228(3)
α [deg]	90	79.240(2)	90
β [deg]	91.633(2)	77.369(2)	94.1120(10)
γ [deg]	90	69.907(2)	90
V [Å^3]	5868.2(4)	2397.9(8)	4119.26(12)
formula units/cell	4	2	4
ρ_{calc} [g cm^{-3}]	1.498	1.541	1.506
μ [mm^{-1}]	0.798	0.722	0.705
θ_{max} [deg]	31.53	31.54	31.52
reflns collected	88 965	31 446	61 593
indep reflns [R(int)]	18 964 [0.0822]	12 463 [0.0693]	13 254 [0.0735]
obsd reflns, $F_o > 4\sigma(F_o)$	15 099	10 305	10 173
abs correction	*SADABS* (Bruker)	*SADABS* (Bruker)	*SADABS* (Bruker)
transm min/max	0.7022/1.0000	0.6268/1.0000	0.5300/1.0000
data/restraints/param	18 964/0/705	12 463/0/516	13 254/0/538
GOF on F^2	1.065	1.028	1.023
final R1, wR2[b] [$I > 2\sigma(I)$]	0.0430, 0.0916	0.0473, 0.1233	0.0428, 0.1092
final R1, wR2[b] [all data]	0.0616, 0.0994	0.0577, 0.1304	0.0612, 0.1189

facial fashion. For the particular case of **4**, this flexibility leads to four different isomers, **4a**−**d**, which are drawn in Chart 1. From now on, the nomenclature used to name isomers where the bpea ligand acts in a facial fashion will consider the relative position of the Ru−Cl bond with regard to the Ru−$N_{aliphatic}$ bond of the bpea ligand. Therefore, isomer **4a** will be named *trans*,*fac*, whereas **4b** will be the *cis*,*fac* isomer. On the other hand, when the bpea ligand acts in a meridional manner, we consider the relative orientation of the ethyl group of the bpea ligand with regard to the Ru−Cl bond, and thus we can have the *mer(down)*-**4c** and *mer(up)*-**4d** isomers depicted in Chart 1. The reaction of **2** with dppe, as described in the Experimental Section, generates a mixture of three of the four geometrical isomers that can be potentially obtained in a molar ratio of 3.3:1.9:1.0 for **4a**/**4b**/**4c** with an overall yield of 51.8%. The remaining dppe ligand produces the neutral $[RuCl_2(dppe)_2]$ complex as a side product. Column chromatography allows the separation of facial from meridional isomers, whereas for the separation of the two facial isomers, a preparative thin-layer chromatography is needed.

The crystal structures of complexes **3**, **4a**, and **4b** have been solved by X-ray diffraction analysis. Their main crystallographic data are reported in Table 1, together with selected bond distances and angles, which can be found in Table 2, and their ORTEP plots, which are depicted in Figure 1. Compound **3** crystallizes in the centrosymmetrical space group $P2_1/c$ with two independent molecules of the complex

Table 2. Selected Bond Distances and Angles for X-ray Structures of **3** (Molecules A and B), **4a**, and **4b** and Calculated Structures **4a**−**d**

bond/angle	**3** (exp)	bond/angle	**4a** (exp)	**4a** (calc)	**4b** (exp)	**4b** (calc)	**4c** (calc)	**4d** (calc)
Ru1A−N3A	2.0506(19)	Ru1−N3	2.1365(18)	2.135	2.1393(18)	2.138	2.097	2.105
Ru1A−N1A	2.084(2)	Ru1−N1	2.1389(16)	2.126	2.0732(17)	2.092	2.109	2.122
Ru1A−N2A	2.1859(19)	Ru1−N2	2.1724(17)	2.206	2.2034(17)	2.236	2.208	2.215
Ru1A−P1A	2.3137(6)	Ru1−P1	2.3026(6)	2.346	2.3069(5)	2.327	2.326	2.347
Ru1A−Cl1A	2.4302(6)	Ru1−P2	2.3067(5)	2.344	2.3271(6)	2.372	2.336	2.356
Ru1A−Cl2A	2.4430(6)	Ru1−Cl1	2.4181(5)	2.418	2.4217(5)	2.425	2.473	2.443
N3A−Ru1A−N1A	81.32(8)	N3−Ru1−N1	81.16(6)	79.9	84.62(7)	79.2	160.0	156.6
N3A−Ru1A−N2A	81.28(8)	N3−Ru1−N2	80.48(7)	79.8	75.89(7)	78.7	80.1	79.4
N1A−Ru1A−N2A	80.96(8)	N1−Ru1−N2	79.38(6)	80.0	81.27(7)	81.0	80.4	77.8
N3A−Ru1A−P1A	99.27(6)	N3−Ru1−P1	177.51(5)	176.1	97.84(5)	97.7	98.4	99.2
N1A−Ru1A−P1A	106.29(6)	N1−Ru1−P1	96.71(5)	96.3	104.08(5)	101.4	100.2	103.2
N2A−Ru1A−P1A	172.75(5)	N2−Ru1−P1	97.88(5)	98.7	171.51(5)	172.3	171.9	175.5
N3A−Ru1A−Cl1A	93.73(6)	N3−Ru1−P2	97.79(5)	98.6	176.47(5)	150.4	93.2	91.2
N1A−Ru1A−Cl1A	167.28(6)	N1−Ru1−P2	176.85(5)	176.5	97.62(5)	101.4	95.6	97.6
N2A−Ru1A−Cl1A	86.73(5)	N2−Ru1−P2	103.42(5)	102.9	101.69(5)	100.4	102.4	99.1
P1A−Ru1A−Cl1A	86.02(2)	P1−Ru1−P2	84.40(2)	85.2	84.30(2)	83.1	85.6	85.1
		N3−Ru1−Cl1	90.59(5)	90.4	89.63(5)	90.7	88.9	91.5
		N1−Ru1−Cl1	93.01(5)	93.3	169.92(5)	165.9	85.0	83.4
		N2−Ru1−Cl1	169.01(5)	169.0	89.32(5)	87.3	85.7	90.2
		P1−Ru1−Cl1	90.82(2)	90.7	84.871(18)	85.9	86.4	85.6
		P2−Ru1−Cl1	84.02(2)	83.5	87.761(19)	88.5	171.9	170.6

in the crystal cell (molecules A and B). The independent molecules differ in the orientation of the phenyl groups of the phosphine ligand. Compounds **4a** and **4b** crystallize as dichloromethane solvates with BF_4^- as the counteranion.

DFT calculations were performed for the four isomers **4a**−**d**. A geometry optimization of the four possible gas-phase isomers was performed. The optimized structures are drawn in Figure 2, and selected bond distances and angles are gathered in Table 2, together with the available experimental counterparts measured at 153 K for the purposes of comparison. The results show a good agreement between the experimental and theoretical data. For isomer **4a**, the standard deviation for the bond distances is 0.019 Å and that for the angles is 0.7°,[18] thus providing confidence in the reliability of the chosen method to reproduce geometries of the studied complexes.

In all cases, the structures of the mononuclear complexes, either the calculated or X-ray diffraction structures, present a distorted octahedral type of coordination with Ru−N, Ru−P, and Ru−Cl bonding parameters in the range of previously reported Ru(II) structures with similar types of ligands.[2b,19] In this set of structures, there are two salient features that are worth mentioning: one is the interligand steric repulsions among aromatic rings of bpea and dppe ligands, and the second is the trans influence exerted by the phosphine ligands.

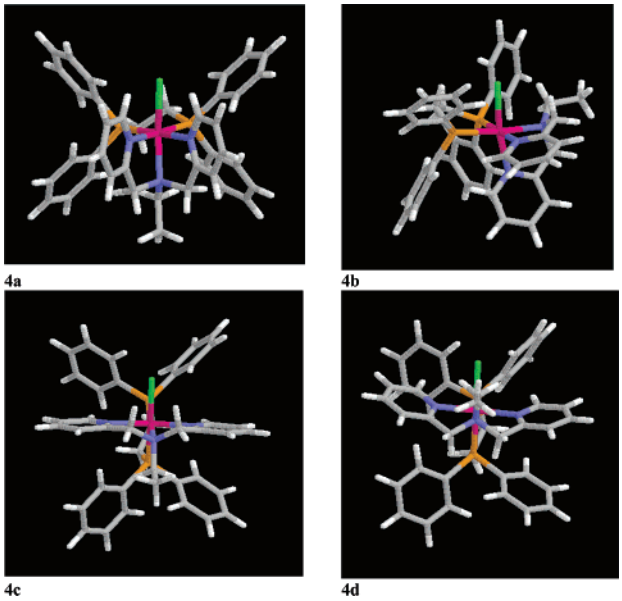

Figure 2. Stick representation of B3PW91-optimized geometries for complexes **4a**−**d**. Color code: Ru, pink; Cl, green; P, orange; N, blue; C, gray; H, white.

To simplify the structural discussion for complexes **4a**−**d**, the plane nearly perpendicular to the Ru−Cl bond, and containing four cis-coordinating atoms with regard to the mentioned Ru−Cl bond, will be considered as the equatorial plane of these molecules. In the *trans,fac* complex **4a** (see Figures 1b and 2), the pyridyl groups are perpendicular to the equatorial plane, a situation that produces relatively small steric interactions between pyridyl−bpea and phenyl−dppe groups. For the *cis,fac* complex **4b**, one of the pyridyl−bpea rings is perpendicular to the equatorial plane, as in the previous case, whereas the second pyridyl is nearly parallel to this plane, producing significant steric interactions with the closest phenyl−dppe rings. In the case of the *mer(down)* complex **4c**, now pyridyl rings are nearly parallel to the equatorial plane and thus produce strong steric interactions with the phenyl−dppe groups. This steric repulsion is even more strongly manifested in the case of the isomer **4d**, where now, as can be inferred from the optimized geometry, the bpea ligand needs to bend in order to reduce steric repulsions (the calculated[17] angles between the best-fitted planes defined by each pyridyl group of bpea are 3.7 and 24.8° for **4c** and **4d**, respectively). The degree of steric repulsions in these isomers is also consistent with the relative energies found for them that are 0.3 (**4b**), 0.8 (**4c**), and 5.3 (**4d**) kcal mol^{-1} above with respect to the energy of isomer **4a**. It is also

(18) The chosen bond distances and angles used for the comparison of the theoretical and experimental data are collected in Table S1 in the Supporting Information.

(19) (a) Romero, I.; Rodríguez, M.; Llobet, A.; Collomb-Dunand-Sauthier, M.-N.; Deronzier, A.; Parella, T.; Stoeckli-Evans, H. *J. Chem. Soc., Dalton Trans.* **2000**, 1689−1694. (b) Polam, J. R.; Porter, L. C. *J. Coord. Chem.* **1993**, *29*, 109−119. (c) Akita, M.; Takahashi, Y.; Hikichi, S.; Moro-oka, Y. *Inorg. Chem.* **2001**, *40*, 169−172.

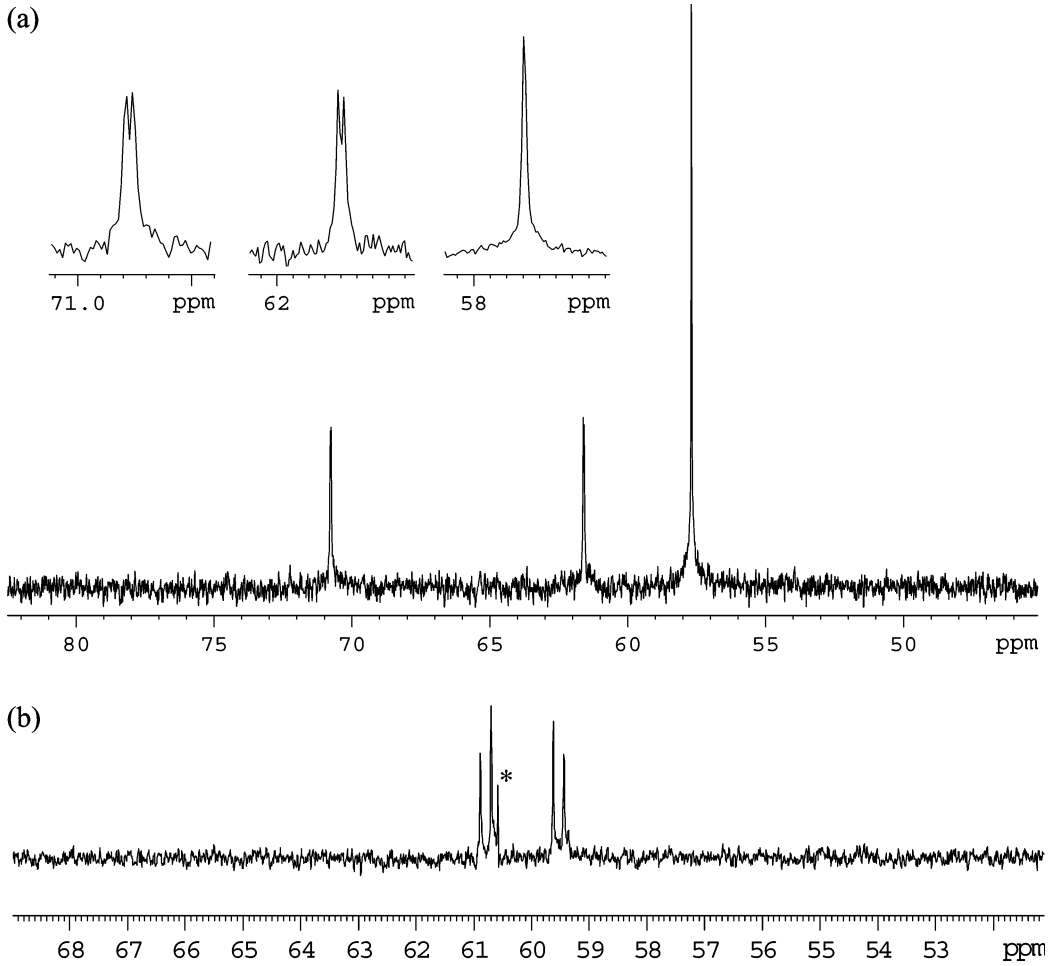

Figure 3. (a) ^{31}P NMR (202 MHz, CD_2Cl_2, 25 °C) spectra for complexes **4a** and **4b**. (b) ^{31}P NMR (101 MHz, CD_2Cl_2, 25 °C) spectra for complex **4c**. The asterisk indicates an artifact signal.

consistent with the relative yields obtained in the synthesis; furthermore, the fact that the isomer **4d** is not observed in the present synthesis is also in agreement with its energy being at least 4.5 kcal mol^{-1} higher with regard to any of the other isomers.

The second interesting characteristic of this set of isomers is the fact that the Ru−Cl bond is trans to bpea N atoms in **4a** and **4b** but trans to dppe P atoms in **4c** and **4d**. The stronger trans influence of the P vs N donor atoms produces a weakening of the Ru−Cl bond that is manifested through the corresponding Ru−Cl bond distances [2.4181(5) Å (exp) and 2.418 Å (calc), **4a**; 2.4217(5) Å (exp) and 2.425 Å (calc), **4b**; 2.473 Å (calc), **4c**; 2.443 Å (calc), **4d**] and that is also consistent with an increase of the Ru(III/II) redox potential by roughly 100 mV for **4c** with regard to either **4a** or **4b** (vide infra), given the decrease of the electron density transferred from the Cl ligand to the metal in **4c** (Mulliken charges for Cl: −0.303, **4a**; −0.307, **4b**; −0.353, **4c**). This trans influence can also be observed for isomers **4a** and **4b** in the Ru1−N2 aromatic bonds [**4a**, Ru1−N2 = 2.1724-(17) Å, Cl trans; **4b**, Ru1−N2 = 2.2034(17) Å, P trans].

It is worth mentioning here that the meridional isomer **4c** constitutes the first example described in the literature of a Ru complex where the bpea ligand adopts this geometry. In all of the Ru−bpea complexes previously described, the bpea ligand adopted a facial geometry.[2d,19a] However, for other transition-metal complexes such as Mn[20,21] and Fe,[22] both meridional and facial geometries had been described.

The increase of steric encumbrance per P atom in PPh_3 with regard to dppe can be held responsible for obtaining a single isomer in the case of the reaction of **1** with bpea, which forms only **3**.

Spectroscopic and Redox Properties. The 1D and 2D NMR spectra of complexes **3** and **4a**−**c** were registered in CD_2Cl_2, are assigned in the Experimental Section, and are shown in Figure 3 and as Supporting Information. All of the NMR resonances for complexes **3**, **4a**, and **4b** can be unequivocally assigned and confirm that their structures in solution are the same as those in the solid state, as was

(20) (a) Romero, I.; Dubois, L.; Collomb, M.-N.; Deronzier, A.; Latour, J. M.; Pécaut, J. *Inorg. Chem.* **2002**, *41*, 1795−1806. (b) Romero, I.; Collomb, M.-N.; Deronzier, A.; Llobet, A.; Perret, E.; Pécaut, J.; Le Pape, L.; Latour, J. M. *Eur. J. Inorg. Chem.* **2001**, 64−72. (c) Dubé, C. E.; Wright, D. W.; Pal, S.; Bonitatebus, P. J.; Armstrong, W. H. *J. Am. Chem. Soc.* **1998**, *120*, 3704−3716. (d) Dubé, C. E.; Mukhopadhyay, S.; Bonitatebus, P. J.; Staples, R. J.; Armstrong, W. H. *Inorg. Chem.* **2005**, *44*, 5161−5175.

(21) (a) Mantel, C.; Hassan, A. K.; Pécaut, J.; Deronzier, A.; Collomb, M.-N.; Duboc-Toia, C. *J. Am. Chem. Soc.* **2002**, *125*, 12337−12344. (b) Pal, S.; Olmstead, M. M.; Armstrong, W. H. *Inorg. Chem.* **1995**, *34*, 4708−4715.

(22) Ito, M.; Takita, Y.-S.; Sakai, K.; Tubomura, T. *Chem. Lett.* **1998**, 1185−1186.

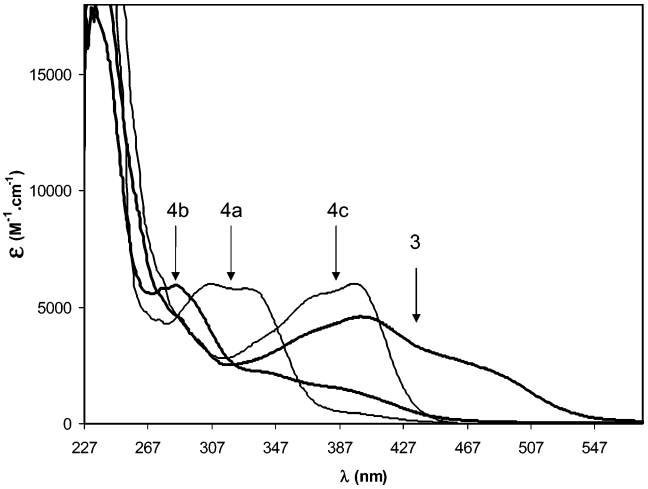

Figure 4. UV/vis spectra for complexes **3** and **4a**−**c**, registered in CH_2Cl_2.

expected for a Ru(II) low-spin d^6 type of metal ion. For complex **4c**, the NMR assignment is fully consistent with the structure obtained via DFT calculations. In particular, the existence of a strong interligand NOE between H13 (from a methylenic bpea) and H16 (from an aromatic dppe) that are situated at 2.147 Å in the **4c** calculated structure (see the Supporting Information for the numbering scheme) and that can be taken as a fingerprint for *mer(down)* type geometry are worth mentioning here because it is not found in either **4a** or **4b** and it is impossible to observe in a potential *mer(up)* **4d** isomer.

Figure 3 shows the ^{31}P NMR spectrum for complexes **4a**−**c**. For the more symmetric isomer **4a**, a singlet is obtained, whereas for **4b** and **4c**, an AB system is obtained in each case because of the nonmagnetic equivalence of the two P atoms of the dppe ligand. The asterisk in Figure 3b indicates an artifact signal because ^1H NMR (see Figure S3b in the Supporting Information) shows that this isomer is highly pure.

The UV/vis spectra of the chloro complexes **3** and **4a**−**c**, registered in CH_2Cl_2, are shown in Figure 4. λ_{max} values, together with the extinction coefficients (ϵ) of **4a**−**c**, are reported in the Experimental Section and summarized in Table 3, which also contains time-dependent DFT (TD-DFT) calculated transitions and the corresponding assignments for experimental and calculated absorptions. All of these complexes present ligand-based $\pi-\pi^*$ transitions at high energies and also bands that can be assigned to a series of metal-to-ligand charge-transfer (MLCT) $d\pi-\pi^*$ (Ru−bpea)[2d] and $d\pi-\pi^*$ (Ru−dppe) transitions at lower energies, vide infra. The energies of the orbitals involved in MLCT transitions are presented in Table 4, and the orbitals involved are displayed in Figure 5 [highest occupied molecular (HOMO) and lowest unoccupied molecular (LUMO) orbitals] and in the Supporting Information.

The LUMO (L) in **4a** presents a strong contribution from the π system of the pyridylic bpea rings and a slight d_{z^2} contribution from the metal center. The L+1 and L+2 orbitals are mainly composed of pyridylic π^* orbitals, whereas both the metal center and the π system of the dppe

Table 3. UV/Vis Spectroscopic Data (in CH_2Cl_2) for Complexes **4a**−**c** Related with MLCT Transitions

complex	experimental λ_{max}, nm (ϵ, M^{-1} cm^{-1})	calculated λ_{max}, nm (associated orbitals)
4a	267 (4684)	275 (H−1 → L+6, L+8)
	303 (5936)	320 (H−2 → L+1, L+2, L+3, L+4)
	334 (5710)	345 (H−2 → L)
4b	276 (5765)	280[a]
	338 (2520)	334 (H−2 → L, L+3)
	343 (2180)	360 (H−2 → L)
	392 (1613)	405 (H, H−1 → L, L+1)
4c	275 (6308)	278 (H → L+3, L+8, L+9)
	335 (3525)	345−358 (H−1 → L, L+3; H−1, H−2 → L+1)
	371 (5499)	375 (H → L; H → L+3)
	396 (6014)	403 (H → L)

[a] Not fully converged.

Table 4. Energy (eV) of Frontier Molecular Orbitals and Other Orbitals Involved in MLCT Bands

orbital	**4a**	**4b**	**4c**
L+3	−3.262	−3.369	−3.363
L+2	−3.667	−3.692	−3.414
L+1	−3.813	−3.900	−3.669
L	−4.106	−4.150	−4.072
H	−7.756	−7.789	−7.947
H−1	−7.876	−7.932	−8.118
H−2	−8.326	−8.534	−8.446
H−3	−8.797	−8.925	−8.870

phenylic rings contribute to L+3. The HOMO (H) for **4a** has a significant d_{yz} participation from the Ru metal in addition to an antibonding contribution from the p_z orbital of the chloro ligand. The H−1 orbital is similar to H but involves the respective d_{xy} and p_x orbitals. Finally, the H−2 orbital is basically the d_{xz} orbital of the metal. The analogous orbitals for the other two isomers, **4b** and **4c**, are also displayed in Figure 5 and in the Supporting Information and are relatively similar to the ones just described for **4a**.

Despite the similarities in the composition of the orbitals just described, it is interesting to note that the H and H−1 orbitals for the meridional isomer **4c** are stabilized by 0.16−0.24 eV with regard to the facial isomers **4a** and **4b** (see Table 4). This stabilization can be understood in terms of the Ru−Cl antibonding interaction in the H and H−1 orbitals and the stronger trans influence exerted by the P atom of the dppe ligand with regard to that of the N atom of the bpea ligand, which produces an elongation of the Ru−Cl bond for **4c** with regard to **4a** and **4b** (see Table 2 for Ru−Cl bond distances). As a consequence of this, the H−L gap for isomer **4c** is 0.225 eV larger than that for isomer **4a**.

As can be seen in Table 3, there is a good agreement between the experimental UV/vis features for isomers **4a**−**c** and those obtained through TD-DFT calculations.[23] However, it is also interesting to note that the energies of the MLCT bands found in the UV/vis spectra for isomers **4a**−**c** do not follow the same trend as the H−L band gap for these isomers. Indeed, as can be seen in Tables 3 and 4, the lowest-energy transitions are paradoxically obtained for the **4c** isomer, which has the largest H−L energy gap. This is due

(23) Silva-López, C.; Nieto-Faza, O.; López, S.; de Lera, A. R. *J. Comput. Chem.* **2005**, *27*, 116−123.

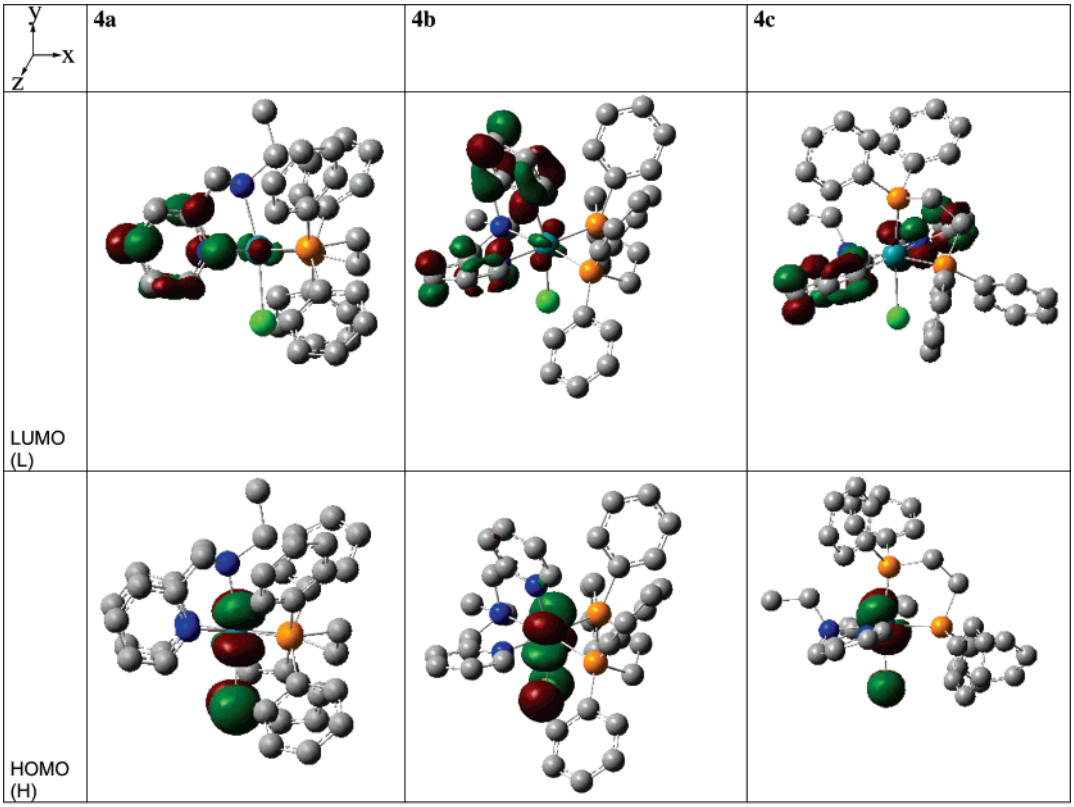

Figure 5. Drawings of HOMO and LUMO orbitals for isomers **4a**−**c** (isosurface values are −0.07 and +0.07 au).

to the fact that, for isomer **4c**, the electronic MLCT originates mainly from the H orbital, whereas for **4a** and **4b**, they involve lower-energy orbitals in the ground state.

The redox properties of the complexes described in the present work were investigated by means of CV techniques. The cyclic voltammograms of **3** and **4a**−**c**, registered in CH_2Cl_2 + 0.1 M TBAP, exhibit chemically reversible and electrochemically quasi-reversible waves assigned to the corresponding Ru(III/II) couples. For the dichloro complex **3**, this wave appears at $E_{1/2} = 0.30$ V vs SSCE ($\Delta E_p = 100$ mV), whereas for the monochloro facial complexes **4a** and **4b**, this wave is anodically shifted to $E_{1/2} = 1.10$ V ($\Delta E_p =$ 150 mV), as was expected from the stronger electron-withdrawing capacity of the diphosphine ligand with regard to the monophosphine. For the meridional complex **4c**, this wave is further shifted to $E_{1/2} = 1.21$ V ($\Delta E_p = 160$ mV), in agreement with the stabilization of the HOMO orbital due to the trans influence described in the previous section, which weakens and thus also labilizes this Ru−Cl bond with regard to the same bond in the facial isomers.

Catalytic Properties. The catalytic properties of complexes **3** and **4a**−**c** were tested with regard to their capacity to perform H-transfer types of reactions between alcohols and aromatic ketones such as acetophenone (AP) and 2,2-dimethylpropiophenone (DP):

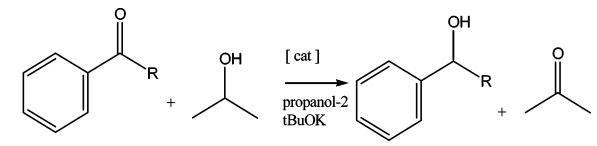

R = Me (AP) or ^{t}Bu (DP)

Table 5. Catalytic Transfer Hydrogenation of Aromatic Ketones[a]

	R	3	4a	4b	4c
1 h	Me	69.3	11.2	23.0	79.3[b]
	^{t}Bu		9.7	13.9	30.0
24 h	Me	99	67.8	26.8	79.3 (0.9)[c]
	^{t}Bu		34.8	18.6	42.0 (3.0)[c]

[a] Percent yield. Experimental conditions: 160:1:80 substrate/catalyst/base. $T = 80$ °C. See the Experimental Section for further details. [b] This conversion value is achieved during the first 14 min. [c] Values in parentheses are obtained under exactly the same conditions except at room temperature.

A preliminary account of these results is presented in Table 5, where the H-transfer reactions are presented at 1- and 24-h reaction times. For the AP case, a first glance at the 24-h reaction time clearly shows that the $RuCl_2$ complex **3** performs excellently and that the performance of the Ru−Cl complexes **4a**−**c** depends strongly on the isomer used. Table 5 also shows that when DP is used as the substrate, the overall yields strongly decrease because of the steric encumbrance of the ^{t}Bu group with regard to that of Me. It is also very interesting to observe here that, for both substrates at the 1-h reaction time, the yields increase in the order **4a** < **4b** < **4c**, which correlates with the degree of steric accessibility of the Ru−Cl bond zone (see structures in Figures 1 and 2). Furthermore, it is also in agreement with a weaker Ru−Cl bond for **4c**, as described in the previous sections. These effects are so dramatic for **4c** that (a) at 1-h reaction time the yields are even better than those for **3** and (b) the H-transfer reaction for both substrates significantly proceeds even at room temperature and the yield is higher for the DP substrate than for AP. The latter is an extremely interesting result because there are very few catalysts that

are capable of performing the H-transfer reaction of bulky ketones in such mild conditions.[24]

Conclusion. In conclusion, the present work shows how simply modifying the ligand coordination geometry can influence both steric and electronic properties and the dramatic impact that these effects have on the reactivity of the complex. Further reactivity work is in progress in our laboratories in order to carry out a comprehensive kinetic study to elucidate reaction pathways and to try to characterize reaction intermediates.

(24) (a) Hashiguchi, S.; Fujii, A.; Takehara, J.; Ikariya, T.; Noyori, R. *J. Am. Chem. Soc.* **1995**, *117*, 7562−7563. (b) Hashiguchi, S.; Noyori, R. *Acc. Chem. Res.* **1997**, *30*, 97−102. (c) Casey, C. P.; Johnson, J. B. *J. Org. Chem.* **2003**, *68*, 1998−2001. (d) Shan, N.; Adams, H.; Thomas, J. A. *Inorg. Chim. Acta* **2006**, *359*, 759−765.

Acknowledgment. This research has been financed by MEC of Spain through Projects BQU2003-02884, CTQ2005-08797-C02-01, BQU2003-01677, and CSD2006-0003. J.M. and A.P. are grateful for the allocation of doctoral grants from the Generalitat de Catalunya and MEC, respectively. A.L. and I.R. also thank Johnson and Matthey for a $RuCl_3 \cdot 3H_2O$ loan.

Supporting Information Available: Additional spectroscopic and computational data (*xyz* coordinates, the main orbitals involved in the less energetic transitions of the UV/vis spectra, and details of the TD-DFT calculations) for the complexes described in this work as well as crystallographic information in CIF format (CCDC 602133−602135). This material is available free of charge via the Internet at http://pubs.acs.org.

IC061126L